DOI: 10.1002/adma.200803341

Correlating Nanomorphology with Charge-Transport Anisotropy in Conjugated Polymer Thin Films

Y. F. Huang, C. W. Chang, D.-M. Smilgies, U. S. Jeng, A. R. Inigo, J. D. White, K. C. Li, T. S. Lim, T. D. Li, H. Y. Chen, S. A. Chen, W. C. Chen and W. S. Fann

Supplementary Material

1 Measurements of Film Homogeneity

Film uniformity was characterized by means of Atomic Force Microscopy (AFM) and optical techniques. The topography of the ~100nm thick spin-coated films formed from both toluene and chlorobenzene were flat having a similar surface roughness of less than 0.4 nm over a 0.25 μm^2 square region with a grain size of ~20 nm (Supplementary Fig. *S1*). The drop cast film was also flat having a surface roughness of 0.7 nm over the same region – quite good considering its much greater thickness (~3.4 μm, Supplementary Fig. *S1c*). (For topographic measurements, MEH-PPV was spin-coated on both pre-cleaned ultra flat ITO coated glass (CEC100S, Präzisions Glas & Optik GmbH) and highly oriented pyrolytic graphite (HOPG, Structure Probe Inc.). Atomic force microscopy (AFM) images were obtained in ambient conditions using a Multimode AFM (Veeco Metrology) equipped with a Nanoscope IV controller (Veeco) using RTESP n-doped Si probes (Veeco, force constant 20 N/m, resonant frequency 300 kHz). Images presented in the paper were plane-fitted and FFT-filtered to remove the 60-Hz noise.)

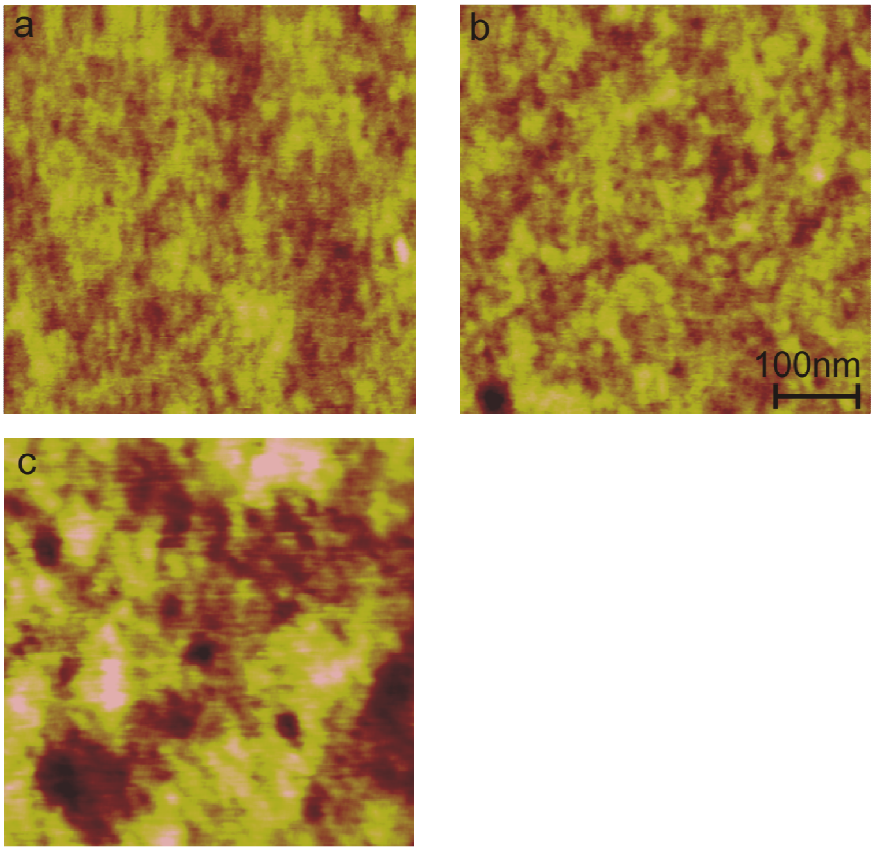

Fig. *S1* AFM topography images (500nm × 500nm) of ~80nm thick films spin cast on ultraflat ITO. (a) Spin cast from chlorobenzene solvent, (b) Spin cast from toluene solvent. (c) Drop cast from chlorobenzene solvent. The corresponding rms surface roughnesses over the 0.25 μm^2 square region were 0.35 nm, and 0.38 nm and 0.72 respectively. The height scale is 5nm in all images.

Film homogeneity was also investigated optically over a larger area by monitoring the photoluminescence (PL) by means of confocal microscopy (40μm × 40μm with ~350nm resolution, Supplementary Fig. *S2*) and nearfield optical microscopy (5μm × 5μm with ~100nm resolution, Supplementary Fig. *S3*) . On these larger length scales, PL was found to be uniform in both intensity and spectral composition across the films (Supplementary Fig. *S4*). In combination the PL images suggest that the distribution of optically active material is homogeneous for all films, not only below, but also above the classical diffraction limit.

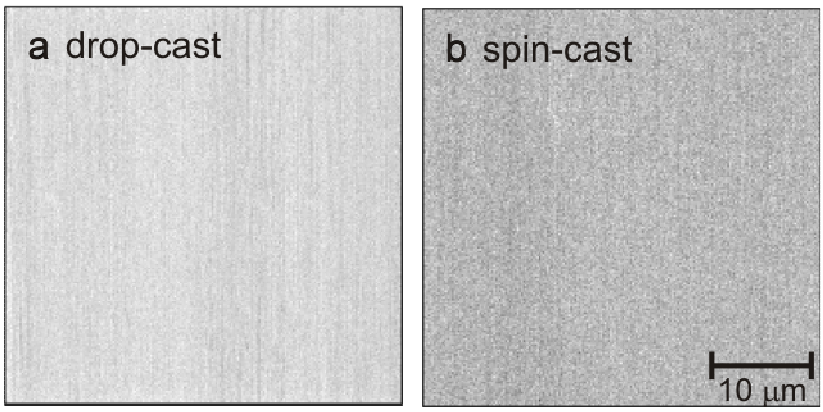

Fig. *S2* Photoluminescence images of MEH-PPV films. Scanned area was 40 μm × 40 μm, excitation wavelength was λ_{exc}= 460 nm, and fluorescence wavelengths beyond 515 was used for imaging. Both excitation and detection bandwidths were chosen for maximized signal-to-noise ratio. (a) drop-cast (~4 μm thick) from chlorobenzene. (b) spin-coated (~80nm thick) from chlorobenzene

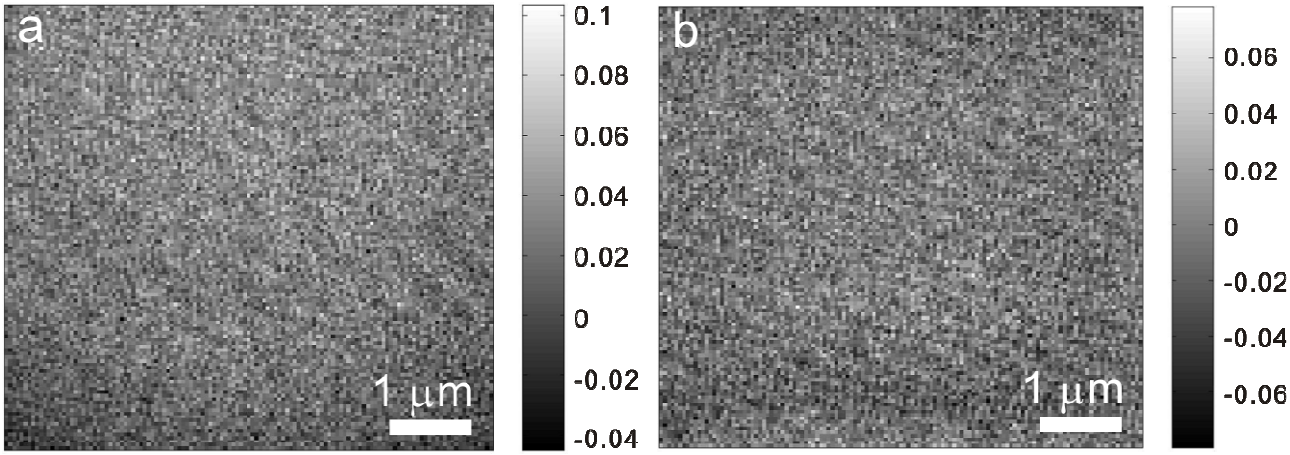

Fig. *S3* Near field optical images of spin-coated films prepared from (a) chlorobenzene and (b) toluene solutions. Images were taken under vacuum conditions to avoid photobleaching. Excitation was at 488nm and observation was at 590 nm. The scale bar in the lower right corner of the figures represents 1 μm. PL images taken at 630nm exhibited a similar lack of contrast supporting that the films are essentially homogeneous.

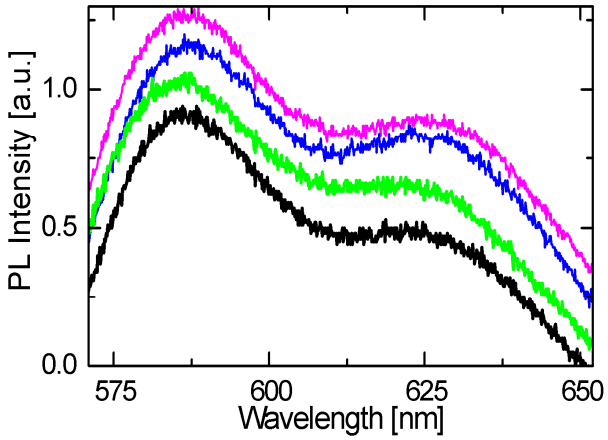

Fig. *S4* Local PL spectra of MEH-PPV thin film spin-coated from chlorobenzene at four different positions on the sample surface. Spectra are recorded in a low pressure nitrogen environment using a homebuilt near field optical microscope. The green, blue and magenta curves are presented offset for clarity. The recorded spectra are independent of position.

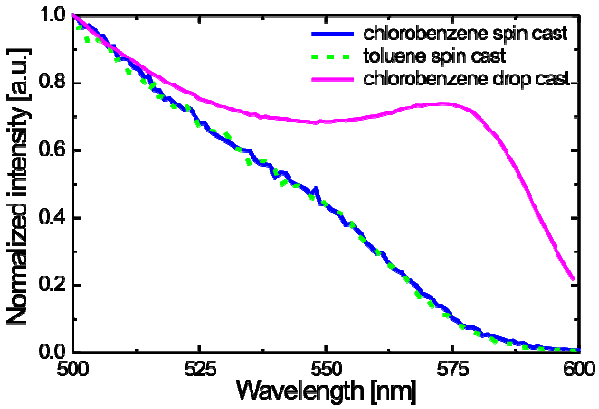

Fig. *S5* Photoluminescence excitation (PLE) spectra monitored at 625 nm for the films spin-coated from chlorobenzene (solid dark blue curve) and toluene (dashed green curve) along with the film drop cast from chlorobenzene (solid magenta curve).

2 Measurements of Mobility in Vertical and Horizontal Directions

Fig. *S6* presents typical raw data used in the determination of transit time yielding the mobility in the diode configuration. In Fig. *S6*a the transit –time electroluminescence (Tr-EL) curves of the two spin-coated films are plotted in linear-log plot. All the transients have similar features: 1) an initial delay time, 2) a fast rise time, 3) a slow rise time to saturation, 4) a fast decay time (after turn-off) and finally 5) a slow decay time back to zero. While much more information

can be extracted from this graph, in the present study we will focus on the delay time, in order to derive the field dependent mobility. Firstly, the initial delay time for the toluene device, corresponding to the transit time for the charge carriers (Fig. *S6*a, $t_{d\text{-}TL}$), is less than that of the chlorobenzene device (Fig. *S6*a, $t_{d\text{-}CB}$). Secondly, the rise time of the toluene device is also much faster than for the chlorobenzene device. Both observations show that the toluene device is performing better than the chlorobenzene device. For comparison, Fig. *S6*b presents the profile of the photo current versus time for the thicker drop cast film from chlorobenzene solution, obtained with the time-of-flight (TOF) technique. The transition time (t_{CB} in Fig. *S6*b) is estimated from the intersections of the two slopes to be ~0.92ms corresponding to a mobility of ~2.5×10^{-6} cm^2/Vs. The above delay times for the spin-coated devices correspond to mobilities of ~10^{-7} cm^2/Vs (chlorobenzene) and 1.6×10^{-6} cm^2/Vs (toluene). The mobility of the spin-coated chlorobenzene based devices is an order of magnitude lower than for the toluene-based device, while the mobility in the chlorobenzene drop-cast device exceeds the ones for the spin-coated devices. (i.e. $\mu_{CB\text{-}spin} < \mu_{TL\text{-}spin} < \mu_{CB\text{-}drop}$). This relationship held at all levels of electric field strength for which measurements were performed.

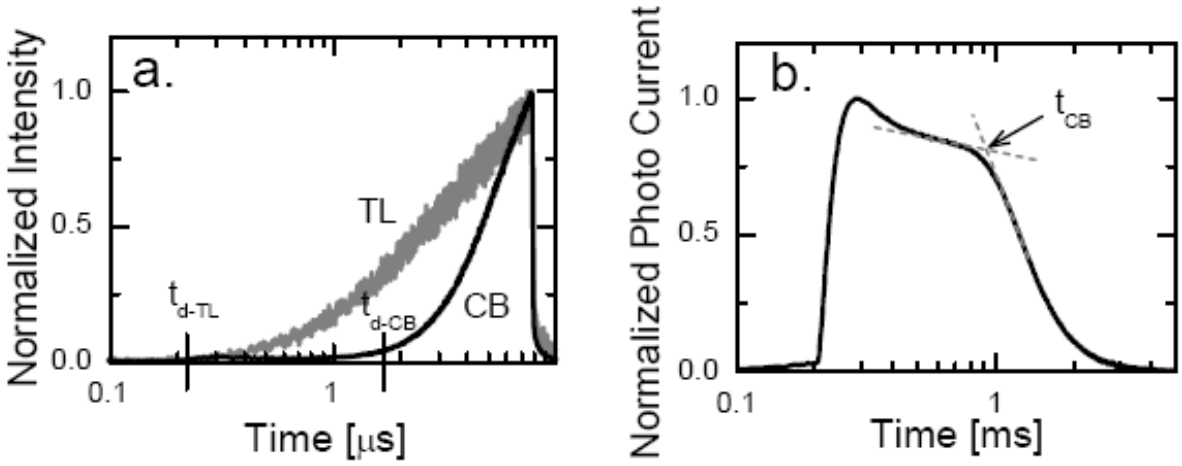

Fig. *S6* Delay and transit times in the diode configuration at 295 K (a) Tr-EL signal in linear-log plot for spin-coated films (~80nm thick) prepared from chlorobenzene and toluene solvents. An electric field of 1.8 MV/cm was applied across the sample. The delay times for the two solvents are indicated by t_{d-CB} and t_{d-TL} for chlorobenzene and toluene respectively. (b) Time of flight (TOF) profile in linear-log plot of the drop cast film (~ 3.4 μm) prepared from CB solution at an applied electric field of 89 kV/cm. The hole transit time is indicated by t_{CB}

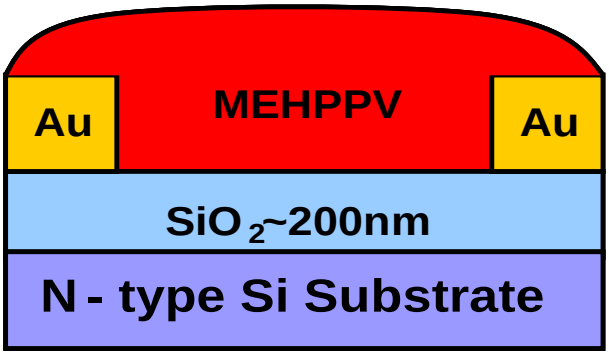

Fig. *S7* Schematic of the bottom contact polymer field effect transistor architecture used for both spin- and drop-cast devices. The channel length and width in this device are 30μm and 1.5 mm, respectively. The bottom contact configuration was chosen to ensure that differences in measured mobility between drop and spin-coated films was solely due to horizontal transport between the electrodes (i.e. in a top contact device carriers in the 4000 nm thick drop cast film must move 8000nm in a vertical direction resulting in a convolution of horizontal and vertical mobility.)

Figure *S8* presents typical data used for the calculation of mobility in the FET configuration. Figure *S8*a shows the measured I-V curves along with the dependence of current on gate voltage (V_g) in the saturation regime for the two spin-coated devices. In both devices the maximum current is of the order of 1 μA. The threshold voltage (V_t) for the two devices is a few volts as determined by linearly fitting ($I_d^{1/2} - V_g$) for voltages ranging from -30 to -100 V under saturation conditions (Fig *S8*b open symbols). The on-off ratio, as shown in I_d vs. V_g, exceeds four orders of magnitude in both devices (Fig. *S8*b solid symbols). The saturation mobilities (under the condition $V_g = V_d = -100$ V) for the two devices were 2.4×10^{-4} cm^2/Vs and 9.4×10^{-4} cm^2/Vs for films spun from toluene and chlorobenzene solutions, respectively. For comparison, the saturation mobility for the drop-cast device formed from chlorobenzene was only ~3×10^{-6} cm^2/Vs. The mobility of the spin-coated toluene devices is lower than for the chlorobenzene devices while the mobility in the chlorobenzene drop cast device is less than that measured in either spin-coated device. (i.e. $\mu_{CB\text{-}spin} > \mu_{TL\text{-}spin} > \mu_{CB\text{-}drop}$). This relationship held at all levels of the electric field used in the measurements.

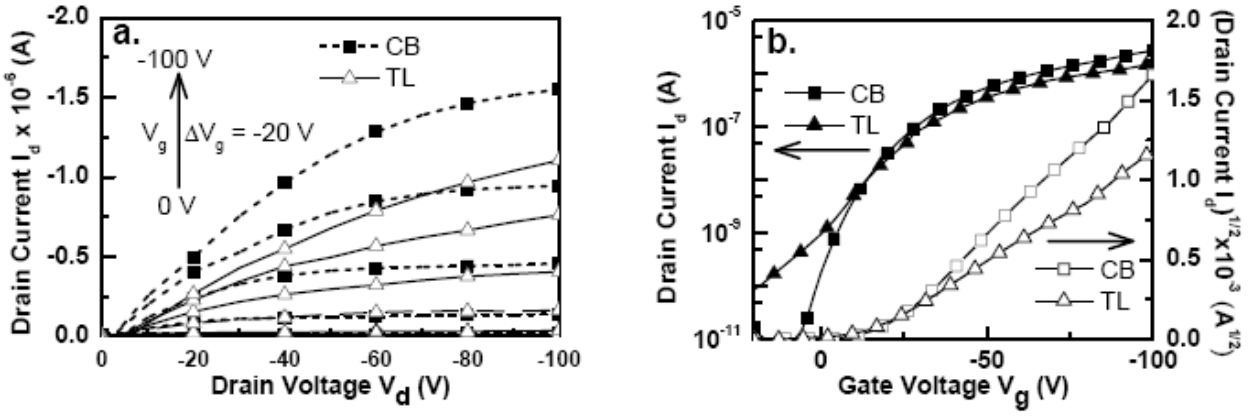

Fig. *S8* Current-Voltage relationships for the FET devices. (a) I-V characteristics of the devices made from chlorobenzene (squares) and toluene (triangles) solutions. The gate voltage (V_g) is varied from 0 to -100 V and plotted with an interval of -20 V. (b) I_d vs. V_g in the saturation regime (V_d =-100V; solid symbols). The open symbols show the square root of the current vs gate voltage to determine the threshold voltage V_t (-10.7 V for chlorobenzene and -6.2 V for toluene devices).

3 GI-WAXS Data

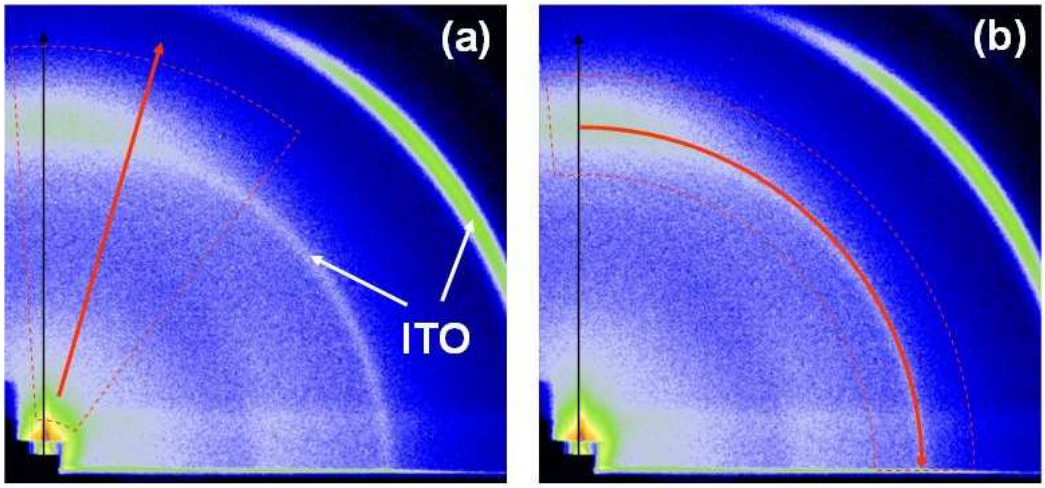

Fig *S9*. Integration areas for radial scans and azimuth scans, as obtained from the CCD scattering image of the CB-spun film. In order to maximize the q-range accepted by the CCD, only half of the full scattering pattern was detected. The corresponding integration areas are indicated by red dashed lines in (a) and (b), while the scan direction is indicated by the red arrow. The MEH-PPV (100) reflection is very broad and peaked around the surface normal indicated by the black arrow. The two sharp powder rings are due to the ITO substrate. The associated integrated scans are provided in Fig 3 a,b of the main paper.

	Average domain size	Texture
CB spin	1.4 nm	+/- 26.8°
TL spin	1.2 nm	+/- 27.5°
CB drop	1.0 nm	+/- 31.4°

Table *S1* Average domain size and texture found for spin-coated (CB spin, TL spin) and drop-cast (CB drop) MEH-PPV films. Values were obtained by fitting the integrated scans in Fig. *3*. Lorentz and Gauss lineshapes yielded consistent values for the half widths. Domain sizes were determined from the width of the backbone ordering peak at 15 nm^{-1} via the Scherrer formula.

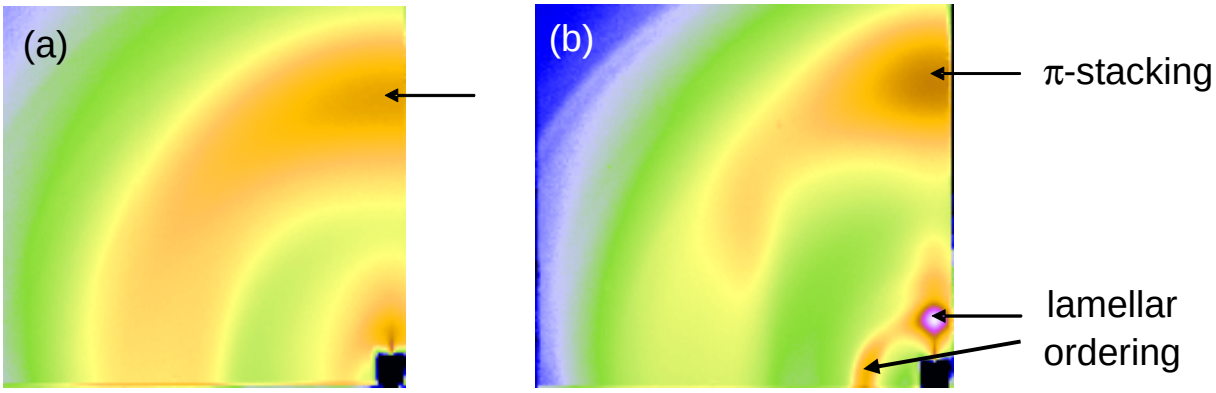

Fig. *S10*. GI-WAXS images of MEH-PPV films spin-coated onto HMDS coated oxidized silicon substrates before (a) and after (b) thermal annealing. The structure before annealing is similar to films spin-coated on ITO coated glass (Fig. 3b-inset in the main paper). The π-stacking of the backbones vertical to the substrate (top arrows in (a) and (b)) is already formed after casting, but the lamellar order only develops after annealing. In the annealed film both parallel lamellae (upper arrow of lamellar ordering) and vertical lamellae (lower arrow of lamellar ordering) coexist. See also H. Sirringhaus et. al. (Nature **1999**, *401*, 685) and H. Yang et al. (Appl. Phys. Lett. **2007**, *90*, 172116).

4 X-ray Reflectivity

In order to determine whether the thickness of this layer was dependent on the thickness of the film, similar XRR data was taken for films of different thicknesses of films spun from chlorobenzene (Fig. *S11*). For all films the Kiessig fringes were found to be modulated and a simulation assuming a ~5nm layer of slightly higher density at the film-substrate interface accurately reproduced the experimental data.

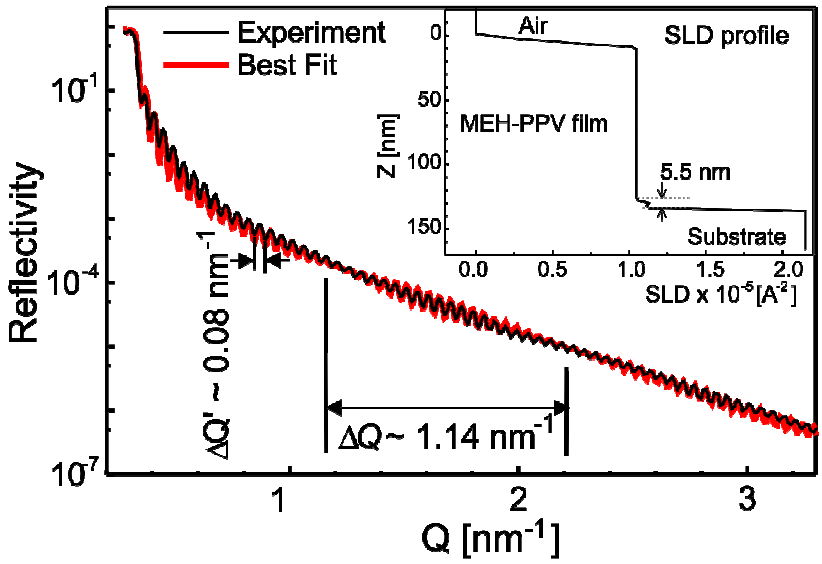

Fig. *S11* X-Ray reflectivity profile of a thick MEH-PPV film spin-coated from chlorobenzene. ΔQ' is the period of the Kiessig fringes indicating that the film's thickness is 132 nm. ΔQ is the period of amplitude modulation of the Kiessig fringes. The dark line represents the experimental data, while the red line shows the simulated XR curve based on the best fit scattering length density (SLD) profile shown in the inset

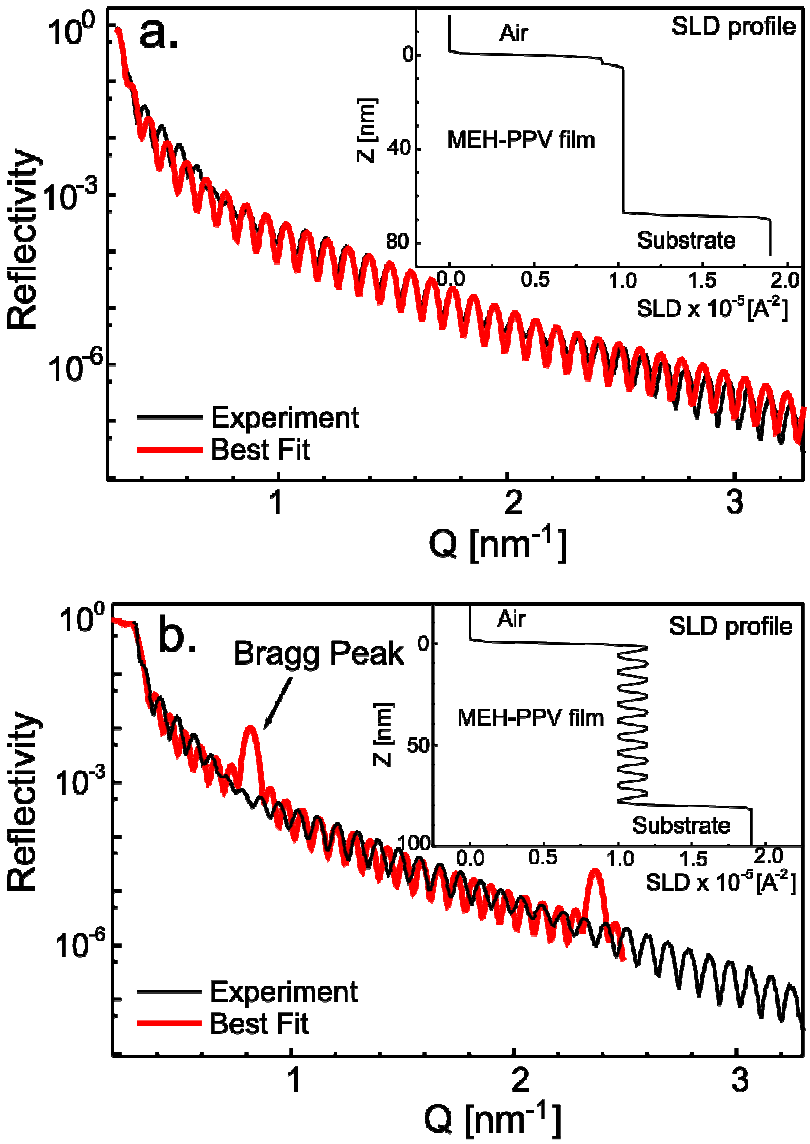

Fig *S12* Other considered models of the XR data from MEH-PPV thin film spin-coated from chlorobenzene. In all figures the dark line represents the experimental data while the red line indicates the predicted fringe modulation for the electron scattering length density (SLD) structure shown in the insets. Rejected models: (a) thin high density layer at the film-air interface (amplitude fits correctly but no modulation of the Kiessig fringes) (b) Alternating layers of high and low electron density (magnitude fits and Kiessig fringes are modulated but Bragg peaks predicted)